Title
A Probe for the Detection of Hypoxic Cancer Cells

Journal
ACS Sensors, 2(8)

ISSN
2379-3694

Authors
Luo, Shenzheng
Zou, Rongfeng
Wu, Junchen
et al.

Publication Date
2017-08-25

DOI
10.1021/acssensors.7b00171

Peer reviewed

ACS SENSORS

Article

pubs.acs.org/acssensors

A Probe for the Detection of Hypoxic Cancer Cells

Shenzheng Luo,[†] Rongfeng Zou,[‡] Junchen Wu,*[,†,§] and Markita P. Landry*[,§,∥]

[†]Key Laboratory for Advanced Materials & Institute of Fine Chemicals, School of Chemistry and Molecular Engineering, East China University of Science and Technology Shanghai 200237, China

[‡]Division of Theoretical Chemistry and Biology, School of Biotechnology, KTH Royal Institute of Technology, SE-10691 Stockholm, Sweden

[§]Department of Chemical and Biomolecular Engineering and [∥]California Institute for Quantitative Biosciences (qb3), University of California Berkeley, Berkeley, California 94720, United States

Supporting Information

ABSTRACT: Hypoxia is a common feature of tumor cells. Nitroreductase (NTR), a common biomarker of hypoxia, has been widely used to evaluate the extent of tumor hypoxia. In this study, three fluorescent probes (FBN-1−3) were synthesized to monitor the extent of hypoxia in cancer cells in real time. FBN-1−3 were composed of a fluorescein analogue and one of three different aromatic nitro groups. Of these probes, FBN-1 showed excellent sensitivity and selectivity in detecting hypoxia via a reduction in O_2 concentration. Confocal fluorescence imaging and flow cytometry demonstrated that HepG-2, A549, and SKOV-3 cells incubated with FBN-1 under reduced oxygen conditions showed significantly enhanced fluorescence. A mouse HepG-2 tumor model confirmed that FBN-1 responds rapidly to NTR and can be used to evaluate the degree of tumor hypoxia. The changes in intra- and extracellular NTR in tumor cells were also concurrently monitored, which did not reveal a link between NTR concentration and degree of hypoxia. Our work provides a functional probe for tumor hypoxia, and our results suggest the fluorescent response of our probe is due to a decrease in O_2 concentration, and not NTR concentration.

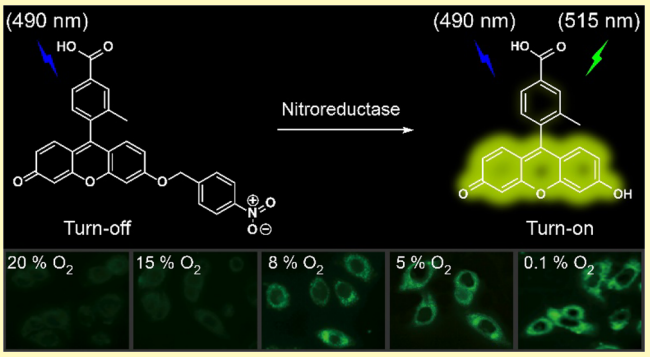

KEYWORDS: *fluorescent probes, nitroreductase, hypoxic fluorescent imaging, tumor detection, hypoxia sensors*

Hypoxia is a pathological condition resulting from the rapid proliferation and vascular abnormalities of tumor cells.[1,2] Hypoxia plays an important role in cancer invasion,[3] metastasis,[4,5] and chemoresistance,[6,7] and has become a primary target in cancer therapy.[1,8−10] The detection of hypoxia is an accurate and reliable method for the diagnosis and treatment of cancer.[11,12] Many intracellular biosubstances have been developed to measure the degree of hypoxia, including nitroreductase (NTR),[13−23] DT-diaphorase,[24,25] and azoreductase.[26,27] Of these biosubstances, NTR is an excellent endogenous molecular biomarker with which to monitor hypoxia because the reaction limit of NTR-catalyzed one-electron reduction is influenced by the oxygen concentration in hypoxic tumor cells or tissues.[28−30] We can group NTR into two categories (oxygen-insensitive and oxygen-sensitive) based on NTR ability to reduce nitro groups in the presence of oxygen or not. We note that both types of NTR catalyze the biological nitroreduction of nitroarenes and have similar substrates.[31−34]

Many studies have confirmed that nitroaromatic compounds are superior substrates for NTR, with reduced nicotinamide adenine dinucleotide (NADH) as the electron donor, under hypoxic conditions.[35−41] Using this reducing activity, Ma et al. developed a resorufin-substituted phenoxazine derivative for imaging hypoxic tumor cells.[29] Recently, Ma et al. measured levels of NTR in zebrafish, using a commercial enzyme linked immunosorbent assay (ELISA) kit.[35] Moreover, Qian's group,[37−39] Tan's group,[40] and Li's group[41] have reported several fluorescent probes composed of an aromatic nitro group and a fluorescent moiety (naphthalimide, Nile blue, and near-infrared cyanine, respectively). All these probes display high sensitivity for NTR, and their fluorescence increases significantly in the presence of NTR. However, existing NTR probes cannot quantify NTR concentrations between cells or quantify different degrees of hypoxia. Here, we implement a new probe for cellular hypoxia that enables us to quantify the concentration of NTR in hypoxic cancer cells and tumors in conjunction with ELISA. Moreover, via fluorescence bioimaging of the fluorescin probe, we show that our fluorescent probe can elucidate the relationship between intracellular NTR concentrations and the degree of hypoxia in different cell samples.

Received: March 17, 2017
Accepted: July 25, 2017
Published: July 25, 2017

DOI: 10.1021/acssensors.7b00171
ACS Sens. XXXX, XXX, XXX−XXX

Inspired by the high sensitivity and rapid response of NTR probes, we designed and synthesized three fluorescein probes decorated with *para*- (FBN-1), *meta*- (FBN-2), or *ortho*- (FBN-3) nitrobenzyl groups (Scheme 1). We chose fluorescein as the fluorescent moiety because of its high fluorescence quantum efficiency, high extinction coefficient (around 490 nm), and high water solubility under physiological conditions. It has also been widely used in biological imaging.[42,43] In the absence of NTR, these three probes showed almost no fluorescence (φ_f = 0.10) because of their electron-withdrawing nitro groups and intramolecular charge transfer processes. Upon addition of NTR in the presence of NADH, the nitroaromatic moiety of FBN-1 was reduced, with the release of the fluorescein derivative (FD, φ_f = 0.90). Thus, a drastic OFF−ON fluorescence is induced by the electron transfer processes with FBN-1 (Scheme 2).

We measured the NTR levels in different hypoxic cells, and found no significant differences in the NTR levels of these cells. We then used FBN-1 to monitor the intratumoral NTR in real time, to determine the degree of hypoxia in tumor cells and tissues with an *in vivo* fluorescence bioimaging. Our results demonstrate that FBN-1 can be used to monitor the degree of hypoxia in real time both *in vitro* and *in vivo*.

Scheme 1. Synthesis of FBN-1−3

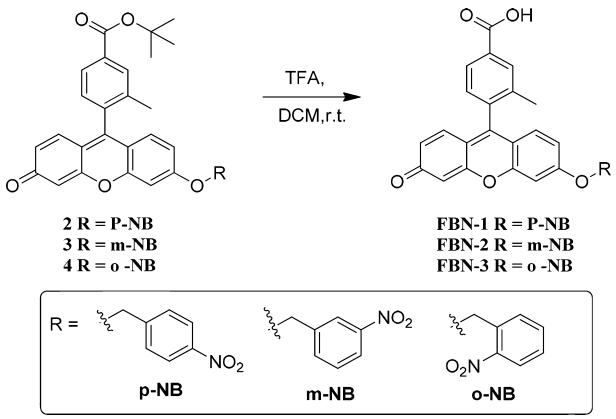

EXPERIMENTAL SECTION

Reagents and Apparatus. 1-(Bromomethyl)-4-nitrobenzene, 1-(bromomethyl)-3-nitrobenzene, 1-(bromomethyl)-2-nitrobenzene, Cs_2CO_3, and KI were purchased from Energy Chemicals. NTR (≥100 units/mg) from *Escherichia coli* and NADH were purchased from Sigma-Aldrich Co. Ltd. (St. Louis, MO, USA). Lysozyme, glutathione reductase (GR), bovine serum albumin (BSA), and DL-dithiothreitol (DTT) were purchased from Sinopharm Chemical Reagent Co., Ltd. Human nitroreductase enzyme-linked immunosorbent assay kit (96t) was purchased from R&D Systems (Minneapolis, USA).

Ultrapure water (18.2 MΩ cm) from the Millipore Filtration System (Milli-Q gradient system, Bedford, MA, USA). ^{1}H and ^{13}C NMR spectra were recorded at room temperature with a Bruker AV 400 spectrometer. Fourier transform infrared (FT-IR) spectra were recorded on a Nicolet 380 FT-IR spectrometer (Thermo Electron Corp.). The UV−vis spectra and fluorescence spectra were recorded with a Varian Cary 100 Conc UV−visible Spectrometer and a Varian Cary Eclipse Fluorescence Spectrometer, respectively. pH was measured with a Mettler Toledo FE 20K pH meter. All melting points were measured with a Bruker Melting-Point B-450 apparatus with an open-ended glass capillary tube. The melting points were not corrected. High-resolution mass spectra were obtained on an LCT Premier XE mass spectrometer (electronic spray ionization, ESI). Flow cytometry experiments were performed with a Millipore Guava flow cytometer (Billerica, MA, USA). A confocal laser scanning microscope (Nikon A1, Japan) was used for the fluorescent imaging of cells and tissue sections.

General Synthetic Procedure for FBN-1−3. Compounds **2**−**4** were synthesized according to the literature (Figures S16−24)[44] with details shown in Scheme S1.

Compound **2** 2.35 g (4.4 mmol) was dissolved in dichloromethane (DCM, 8 mL) and cooled to 0 °C; trifluoroacetic acid (TFA, 8 mL) was added dropwise with stirring, and the solution was stirred for 2 h at room temperature. The reaction was monitored with thin layer chromatography (TLC). After the reaction was complete, the solvent

Scheme 2. Mechanism of FBN-1 Response to Hypoxia

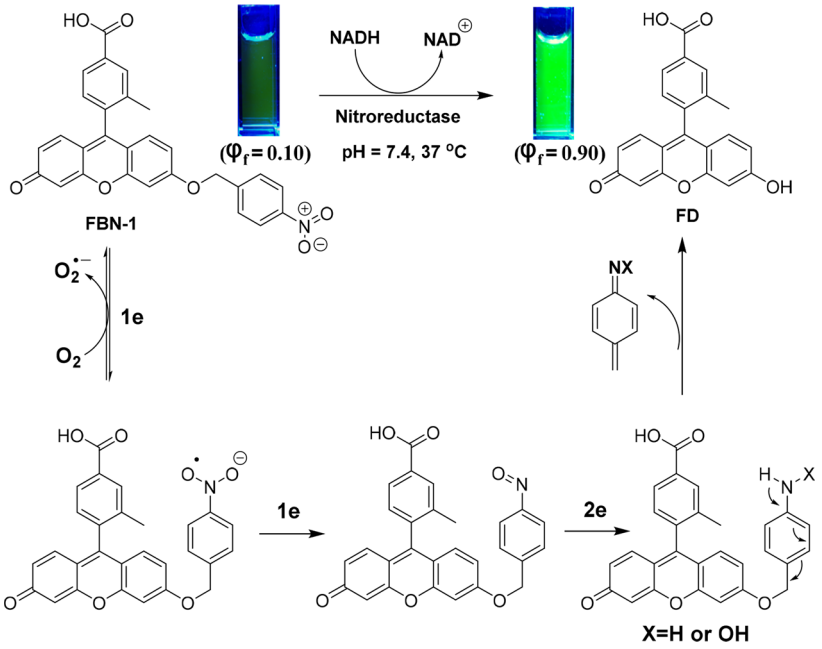

DOI: 10.1021/acssensors.7b00171
ACS Sens. XXXX, XXX, XXX−XXX

was removed and the residue was purified on a silica gel column (DCM/MeOH = 300/1 → 50/1) to produce the compound.

FBN-1: 1.9 g (4.0 mmol, 91%, light yellow solid). ^{1}H NMR (400 MHz, DMSO-d_6) δ 13.23 (s, 1H), 8.29 (d, J = 8.2 Hz, 2H), 8.07 (s, 1H), 7.98 (d, J = 7.8 Hz, 1H), 7.76 (d, J = 8.5 Hz, 2H), 7.43 (d, J = 7.9 Hz, 1H), 7.36 (s, 1H), 7.05 (dd, J = 8.9, 2.1 Hz, 1H), 6.94 (d, J = 8.9 Hz, 1H), 6.87 (d, J = 9.7 Hz, 1H), 6.47 (dd, J = 9.7, 1.8 Hz, 1H), 6.29 (d, J = 1.5 Hz, 1H), 5.48 (s, 2H), 2.09 (s, 3H); ^{13}C NMR (101 MHz, DMSO-d_6) δ 183.9, 166.9, 162.7, 158.1, 153.8, 147.67, 147.1, 143.8, 136.4, 131.8, 131.2, 130.3, 129.9, 129.5, 129.2, 128.4, 127.0, 123.7, 117.4, 114.3, 113.6, 104.9, 101.7, 68.9, 31.3, 19.00; FT-IR: ν [cm^{-1}] 3425, 3062, 2915, 2853, 1705, 1640, 1585, 1490, 1388, 1350, 1255, 1200, 1110, 1025, 913, 840, 740, 600, 490; MS-ESI: m/z calculated for $C_{28}H_{19}NO_7$ [M + H]$^+$ 482.1240, found 482.1238; melting point: 271.5−273.6 °C (Figures S25−27).

FBN-2: 72 mg (0.15 mmol, 78%, light yellow solid). ^{1}H NMR (400 MHz, DMSO-d_6) δ 13.17 (s, 1H), 8.37 (d, J = 1.7 Hz, 1H), 8.24 (dd, J = 8.2, 1.4 Hz, 1H), 8.06 (s, 1H), 7.97 (t, J = 8.4 Hz, 2H), 7.74 (t, J = 8.0 Hz, 1H), 7.44 (d, J = 8.2 Hz, 2H), 7.09 (dd, J = 8.9, 2.2 Hz, 1H), 6.98 (d, J = 9.0 Hz, 1H), 6.92 (dd, J = 9.7, 1.4 Hz, 1H), 6.52 (d, J = 9.7 Hz, 1H), 6.38 (s, 1H), 5.48 (s, 2H), 2.09 (s, 3H); ^{13}C NMR (101 MHz, DMSO-d_6) δ 183.5, 166.9, 163.1, 158.3, 154.1, 148.5, 147.8, 138.3, 136.5, 136.4, 134.2, 132.5, 131.9, 131.2, 130.4, 130.2, 129.5, 129.3, 127.4, 127.0, 123.1, 122.3, 117.4, 114.5, 113.8, 104.8, 101.7, 68.9, 19.00; FT-IR: ν [cm^{-1}] 3435, 2955, 2920, 2855, 1705, 1640, 1600, 1525, 1485, 1390, 1350, 1280, 1250, 1200, 1115, 1025, 905, 850, 735, 665, 605, 540, 495; MS-ESI: m/z calculated for $C_{28}H_{19}NO_7$ [M + H]$^+$ 482.1240, found 482.1239; melting point: 260.1−262.8 °C (Figures S28−30).

FBN-3: 65 mg (0.14 mmol, 71%, light yellow solid). The light was avoided during preparation. ^{1}H NMR (400 MHz, DMSO-d_6) δ 13.21 (s, 1H), 8.18 (d, J = 8.0 Hz, 1H), 8.07 (s, 1H), 7.98 (d, J = 7.7 Hz, 1H), 7.87−7.75 (m, 2H), 7.73−7.62 (m, 1H), 7.45 (d, J = 7.9 Hz, 1H), 7.41 (d, J = 1.5 Hz, 1H), 7.05 (dd, J = 9.1, 2.2 Hz, 1H), 6.96 (d, J = 8.9 Hz, 1H), 6.89 (d, J = 9.7 Hz, 1H), 6.50 (s, 1H), 6.32 (s, 1H), 5.68 (s, 2H), 2.10 (s, 3H); ^{13}C NMR (101 MHz, DMSO-d_6) δ 183.3, 166.9, 163.0, 158.3, 154.2, 148.8, 147.5, 136.5, 134.2, 131.9, 131.3, 131.2, 130.5, 129.6, 129.5, 129.4, 129.3, 127.0, 125.0, 117.5, 114.6, 114.0, 104.7, 101.7, 67.4, 29.0, 19.0; FT-IR: ν [cm^{-1}] 3445, 2955, 2925, 2840, 1705, 1640, 1600, 1525, 1500, 1385, 1335, 1290, 1250, 1200, 1120, 910, 845, 735, 600, 490; MS-ESI: m/z calculated for $C_{28}H_{19}NO_7$ [M + H]$^+$ 482.1240, found 482.1235; melting point: 244.6−246.6 °C (Figures S31−33).

UV−vis and Fluorescence Experiments. Ultrapure water (18.2 MΩ cm) was used to prepare all aqueous solutions. Unless otherwise stated, all the UV−vis spectra and fluorescence spectra were measured in 50 mM Tris-buffered saline (TBS, pH = 7.4) containing 2.5% DMSO, with the following procedure. The TBS and FBN-1−3 solutions were incubated in a gas bath thermostatic oscillator at 37 °C for 30 min before use. In a 1.5 mL tube, 10 μM FBN-1 (0.4 mL) and 2 mM NADH (0.2 mL) were mixed, and then an appropriate volume of oxygen-insensitive NTR was added. The final solution volume was adjusted to 0.8 mL with TBS. The solution was rapidly mixed and subsequently incubated in a gas bath thermostatic oscillator at 37 °C. The solution was then transferred to a 10 × 10 mm^2 quartz cell to measure the absorbance or fluorescence spectrum. The fluorescence spectra were measured ($\lambda_{ex}/\lambda_{em}$ = 490/515 nm) with 5/5 nm slit widths. All the spectra were corrected for intensity with the manufacturer-supplied correction factors and corrected for background fluorescence and absorption by subtracting a blank scan of the buffer system.

Confocal Microscopic Imaging of Cells. HepG-2 (human hepatocellular carcinoma), A549 (human pulmonary carcinoma), and SKOV-3 (human ovarian carcinoma epithelial) cells were seeded in 35 mm Petri dishes with glass cover slides and allowed to adhere overnight before treatment. Cells were then incubated with FBN-1 (5 μm/mL) for 30 min at 37 °C under humidified conditions in 95% air and 5% CO_2, and washed three times with phosphate-buffered saline (PBS). The cells were then kept under normoxic (20% O_2) or different hypoxic conditions (15%, 8%, 5%, or 0.1% O_2), generated with an AnaeroPack (Mitsubishi Gas Corp.)[45−47] for another 8 h at 37 °C. After the cells were washed with PBS (pH 7.4, 1 mL × five times), they were imaged. The fluorescent cell images were obtained with a confocal laser scanning microscope (Nikon A1; 60× oil immersion objective lens). The channel for FBN-1 was excitation at 488 nm and emission collected at 500−550 nm.

Flow Cytometry. The uptake of FBN-1 by the SKOV-3, HepG-2, and A549 cells was measured with a Millipore Guava flow cytometer. HepG-2, A549, and SKOV-3 cells were seeded in six-well plates and allowed to adhere overnight before treatment. The cells were then incubated with FBN-1 (5 μM) for 30 min at 37 °C in humidified conditions under 95% air and 5% CO_2, and washed three times with PBS. Each type of cell was then kept under normoxic (20% O_2) or different hypoxic conditions (15%, 8%, 5%, or 0.1% O_2), for another 8 h at 37 °C. The cells were then washed three times with PBS (pH 7.4), harvested with 0.05% trypsin/EDTA (Sigma), and centrifuged at 117 g for 5 min. The harvested cells were then suspended in PBS (pH 7.4). Each cell type was immediately analyzed with a flow cytometer. The channel for FBN-1 was excitation at 488 nm and emission collected at 510−550 nm. Cells cultured without FBN-1 (control) were prepared for comparison.

ELISA.[35] (1) Sample Preparation. HepG-2, A549, and SKOV-3 cells were cultured without fetal bovine serum under normoxic (20% O_2) or different hypoxic conditions (15%, 8%, 5%, or 0.1% O_2), for 8 h at 37 °C. The cell suspensions were collected and centrifuged at 827 g for 20 min before analysis with an ELISA kit. The cells were harvested with 0.05% Trypsin/EDTA (Sigma) and diluted with PBS (pH 7.4) to a concentration of 10^6 cells/mL. The cell solutions were then lysed via freeze−thawing to release their intracellular components. The lysates were centrifuged for 20 min at 827 g. The cell suspensions were collected and analyzed with an ELISA kit. A 50 mg tumor tissue sample was homogenized and mixed with 1.5 mL of PBS (pH 7.4, 4 °C), ground for 10 min, and centrifuged at 827 g for 20 min. The supernatant was collected and analyzed with an ELISA kit. (2) ELISA Development. The samples (10 μL) were added to 96-well ELISA plates. Next, 40 μL of sample diluent and 100 μL horseradish peroxidase conjugated reagent were added to each well, except the blank wells. The plates were closed with the plate closure membranes and incubated for 1 h at 37 °C. The samples were washed 5−6 times with washing buffer after the plate closure membrane was removed. Chromogen solution A (50 μL) and chromogen solution B (50 μL) were added to each well and left to react for 15 min at 37 °C in the dark. Stop solution (50 μL) was then added to each well to stop the reaction (blue color changed to yellow). The blank well was set equal to zero, and the absorbance of the samples was read at 450 nm with a Multimode Plate Reader (BioTek, USA) within 15 min of the addition of stop solution.

***In Vivo* Fluorescence Imaging.** The mice were imaged using the IVIS Spectrum *in vivo* imaging system (PerkinElmer). The mice were anesthetized with an inhalation of 2% isoflurane for 30 s in an anaerobic box before fluorescence imaging. After an intratumor injection of FBN-1 (0.2 mM) in 0.1 mL of PBS (pH 7.4), the mice were placed in the *in vivo* imaging system (PerkinElmer) for *in vivo* fluorescence imaging ($(\lambda_{ex}/\lambda_{em}$ = 490/520 nm).

RESULTS AND DISCUSSION

Optical Responses of FBN-1−3 to NTR. The spectroscopic properties of the probes (5 μM) were evaluated in TBS (pH 7.4; 2.5% DMSO). All three probes showed two prominent absorption bands centered at 456 and 479 nm (Figure 1a).

The corresponding fluorescence emission maximum was at 515 nm (Figure 1b). Upon addition of oxygen-insensitive NTR in the presence of 500 μM NADH, no change in the absorption spectrum of FBN-2 or FBN-3 was observed. However, with the addition of NTR, the initial absorption bands of FBN-1 at 456 and 479 nm decreased, with the simultaneous emergence of a band centered at 493 nm (Figure 1a). The emission intensity of

DOI: 10.1021/acssensors.7b00171
ACS Sens. XXXX, XXX, XXX−XXX

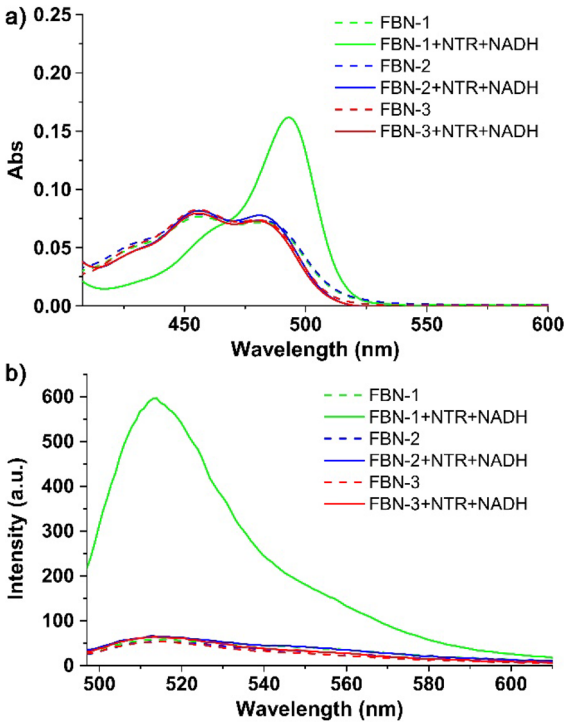

Figure 1. (a) UV–vis and (b) fluorescence spectra of FBN-1, FBN-2, and FBN-3 (5 μM) before and after their reaction with NTR (1 μg/mL) in the presence of NADH (500 μM).

FBN-1 at 515 nm increased significantly, whereas the fluorescence intensity of FBN-2 and FBN-3 remained nearly constant at different concentrations of NTR (Figure 1b). The docking calculations also showed that FBN-1 is an ideal candidate probe for detecting NTR (Figure S1).

Optical Response of FBN-1 to NTR. The selectivity of FBN-1 for NTR was analyzed further. The reactions of FBN-1 with various potential interfering species were examined under the same conditions. As shown in Figure S2a, no significant increase in fluorescence was observed upon FBN-1 exposure with potentially interfering species. In contrast, when FBN-1 was incubated with NTR (0.6 μg/mL) and NADH (500 μM), the fluorescence intensity of FBN-1 increased sharply, showing that FBN-1 is highly selective for NTR over the other species.

The kinetic curves of FBN-1 fluorescence upon reaction with various concentrations of NTR (0, 0.15, 0.3, or 0.6 μg/mL) are shown in Figure S2b. Higher concentrations of NTR result in faster substrate turnover, as shown by faster increases in FBN-1 fluorescence intensity for the initial time points. The time required to reach maximum fluorescence intensity was about 5 min. In contrast, there was no change in the fluorescence intensity within a 10 min period in the absence of NTR. As shown in Figure S3a, the maximum fluorescence intensity of FBN-1 increased as the concentration of NTR increased. The increase in FBN-1 fluorescence showed a linear response to NTR concentration at 0–0.1 μg/mL NTR (Figure S3b). The detection limit for NTR was determined to be 0.66 ng/mL, which is significantly lower than most previously reported NTR probes. This high selectivity for and fast response to NTR indicates that FBN-1 is an excellent probe for rapidly imaging NTR with a dynamic range appropriate for comparing different degrees of hypoxia in biological samples. The above parameters relating to reaction selectivity and *in vitro* FBN-1 reaction rate with oxygen-insensitive NTR provides a reference for the reaction between our probe and NTR in our later experiments.

NTR inhibition with dicoumarin[35] was performed to illustrate the effect of NTR inhibition on FBN-1. When FBN-1 was pretreated with 0.1 mM dicoumarin and then mixed with NTR, the fluorescence intensity was much lower than that without dicoumarin (Figure S4). Moreover, increasing the concentration of dicoumarin to 0.2 mM caused a further decrease in probe fluorescence intensity, which confirmed that the NTR activity of FBN-1 was inhibited by dicoumarin and the fluorescence off–on response of FBN-1 to NTR arose from the NTR-catalyzed reaction.

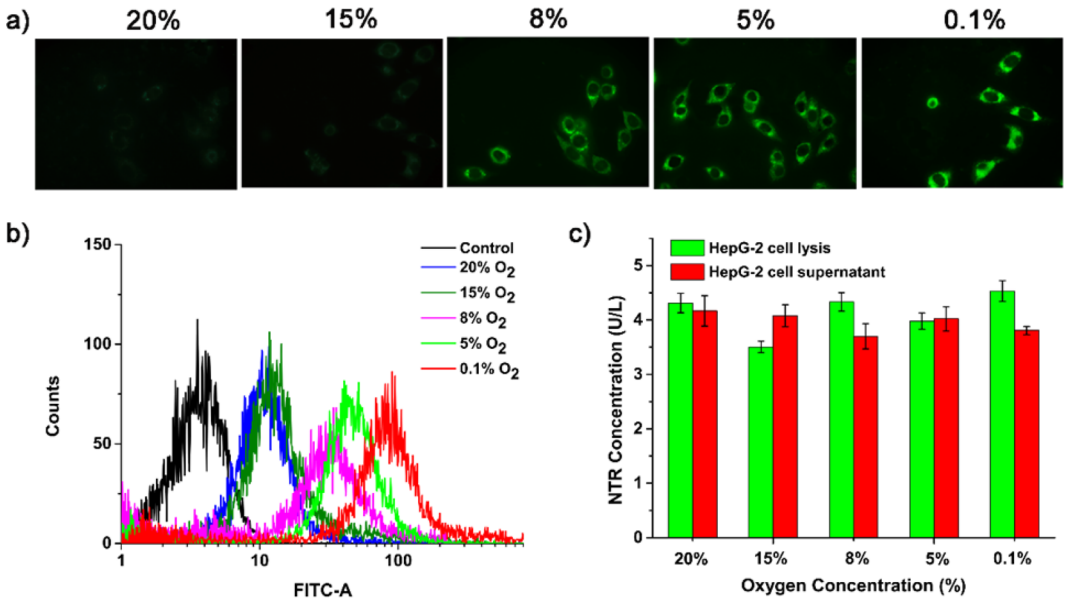

Figure 2. (a) Confocal fluorescence microscopy, and (b) flow cytometric analysis of HepG-2 cells. (c) Quantitative detection of NTR levels in HepG-2 cell lysate and supernatant with ELISA. HepG-2 cells were incubated with FBN-1 (5 μM) under 0.1% O_2, 5% O_2, 8% O_2, 15% O_2, or 20% O_2 for 8 h.

DOI: 10.1021/acssensors.7b00171
ACS Sens. XXXX, XXX, XXX–XXX

Mechanism by Which FBN-1 Detects Hypoxia. In hypoxic tumor cells, NTR catalyzes the one-electron reduction of the nitro group, producing a nitro anion radical. However, the intracellular concentration of oxygen plays an important role in oxidizing the free radical anion to a nitro group.[27,29] Therefore, FBN-1 is expected to detect hypoxia in tumor cells by detecting endogenous NTR. ESI-mass spectrometry (MS) and HPLC analyses were used to verify the sensing mechanism described above. In the ESI-MS spectrum of the reaction solution of FBN-1 and NTR, a major peak was observed at m/z = 347.0919 (Figure S5), corresponding to FD ($[M^+]$ = 347.0922). HPLC was also used to verify these observations. As shown in Figure S6, in the HPLC analysis, there is a weak peak at 17.53 min and a new peak at 15 and 12 min corresponding to standard samples of FBN-1 and FD, respectively. These results support the proposition that the system can be "tuned" by "caging" the FD scaffold.

The reaction might proceed through the route depicted in Scheme 2: the nitro group of FBN-1 is reduced to a nitro anion radical; the nitro anion radical is then reduced to nitroso and hydroxylamine intermediates; the primary amines are the final reduced product in the presence of endogenous NTR and NADH. The unstable *p*-aminobenzyl derivative releases FD and the fluorescence emission is restored.[39] To understand the optical properties of FBN-1, a density functional theory calculation was made at the B3LYP/6-31G* level using a Gaussian 09 program. The results showed a charge transfer from the xanthene π-conjugated moiety to the nitro aromatic moiety in FBN-1, but no charge transfer was detected in FD (Figure S7). This confirms that the intramolecular electron-withdrawing group that induces the electron transfer process occurs in FBN-1, and not in FD. This computed charge transfer is the theoretical basis of the FBN-1 "turn on" property.

Determining the Degree of Hypoxia in Tumor Cells with FBN-1. A 3-(4,5-dimethyl-2-thiazolyl)-2,5-diphenyl-2*H*-tetrazolium bromide (MTT) assay was first used to determine the biocompatibility of FBN-1. FBN-1 showed no cytotoxicity toward HepG-2, A549, or SKOV-3 cells with (Figure S8) or without (Figure S9) irradiation of 490 nm light, confirming the biocompatibility of FBN-1. We then applied FBN-1 to tumor cells to measure their hypoxia *in vitro*. HepG-2, A549, and SKOV-3 cells were chosen as model cell lines because they have been shown to express NTR under hypoxic conditions.[14,29,41,48] Cells were incubated with FBN-1 for 30 min at 37 °C, and then kept under normoxic (20% O_2) or different hypoxic conditions (15%, 8%, 5%, or 0.1% O_2) for another 8 h. As shown in Figure 2a, HepG-2 cells under normoxic conditions showed weak fluorescence, whereas cells incubated under hypoxic conditions showed increasingly strong FBN-1 fluorescence intensities. Thus, the fluorescence intensity of FBN-1 increases as the degree of cellular hypoxia increases. Similar patterns were observed for A549 cells and SKOV-3 cells (Figure S10a,b).

Flow cytometry was used to quantitatively evaluate the differences in fluorescence intensity under normoxic (20% O_2) and different hypoxic conditions (15%, 8%, 5%, or 0.1% O_2). As shown in Figure 2b, the fluorescence intensity did not differ significantly in the HepG-2 cells after incubation under 20% O_2 or 15% O_2, but the fluorescence intensity of the cells was dramatically enhanced in the cells below 8% O_2. Similar flow cytometric results were observed for A549 cells (Figure S11a) and SKOV-3 cells (Figure S11b). These results are consistent with the confocal microscopic imaging of the hypoxic cells, and indicate that FBN-1 is an excellent probe for imaging different levels of tumor hypoxia at the cellular level.

Dicoumarin, an inhibitor of endogenous NTR, was also used to ensure that the fluorescence in the cells incubated with FBN-1 was caused by the NTR-catalyzed reductase reduction. As shown in Figure S12a,b, the fluorescence intensity of either HepG-2, A549, or SKOV-3 cells incubated with dicoumarin was much weaker compared to the fluorescence intensity of the cells without dicoumarin, which indicated that the activity of endogenous NTR in the cells can be inhibited by dicoumarin. It is thus likely that the fluorescence of our cells incubated with FBN-1 is mediated by NTR.

Previous studies have hypothesized that an increase in NTR concentration is a likely reason for the increased fluorescence of fluorescin probes observed under hypoxic conditions.[40,41] Here, ELISA was performed to quantify the expression of NTR in the three tumor cell lines. The NTR concentrations in the cell supernatants or lysates were 4 U/L, 3 U/L, and 2.5 U/L in the HepG-2 (Figure 2c), A549 (Figure S13a), and SKOV-3 cells (Figure S13b), respectively. We found no significant difference in NTR concentrations in the same cell line under different hypoxic conditions (15%, 8%, 5%, or 0.1% O_2). In short, the fluorescence intensity of the probe increased gradually as the oxygen concentration decreased in the cultured cancer cells, but the levels of NTR varied only slightly. In addition, dicoumarin-based NTR inhibition suggests that FBN-1 fluorescence indeed originates from intracellular NTR (Figure S14). Our results suggest that the main reason for the increase in nitroreductase fluorescence is that fewer nitro anion radicals are oxidized to nitro groups under hypoxic conditions.

Determining the Degree of Hypoxia in a HepG-2-Tumor-Bearing Mouse Model. Generally, the larger a tumor, the more severe its degree of hypoxia.[41] To determine the potential utility of FBN-1 *in vivo*, a HepG-2-tumor-bearing mouse was utilized to validate the suitability of FBN-1 for hypoxia bioimaging *in vivo*. Tumors were grown in the living mice for 7 or 35 days via subcutaneous implantation of HepG-2 cells. FBN-1 (0.2 mM, 100 μL in PBS buffer) was then injected into the tumor site. At 1, 5, 10, or 20 min after injection, the net fluorescence intensity increased as shown in Figure 3a, with a leveling of the fluorescence intensity approximately 20 min after the injection of FBN-1 (Figure S15). At fluorescence equilibrium, the fluorescence intensity was nearly twice as high in the 35 day tumor, than the 7 day tumor. After imaging the fluorescence *in vivo*, the tumors were dissected from the mice. The diameters of the 7 day and 35 day tumors were about 6 mm and 14 mm on average, respectively. The fluorescence in the images of the naked tumors was also measured (Figure 3b,c). The average fluorescence intensity of the 14 mm excised tumor was roughly three times greater than the fluorescence intensity from the 6 mm excised tumor. The expression of NTR in solid tumors was quantified with ELISA. The 6 mm and 14 mm solid HepG-2 tumors contained 1.8 and 2.0 U/g enzyme, respectively, indicating that the NTR levels remain unchanged with tumor growth and age. In both our cellular assays (Figure 2) and tumor assays (Figure 3), we find that NTR expression is independent of the degree of hypoxia in these samples, contrary to prior findings.[12−14,35,37,40,41] Our work directly quantifies NTR expression in hypoxic samples, and links NTR expression to degree of hypoxia. These results indicate that our probe may be used to quantify degree of hypoxia in tumors *in vivo*. Furthermore, our results provide preliminary insights suggest-

DOI: 10.1021/acssensors.7b00171
ACS Sens. XXXX, XXX, XXX−XXX

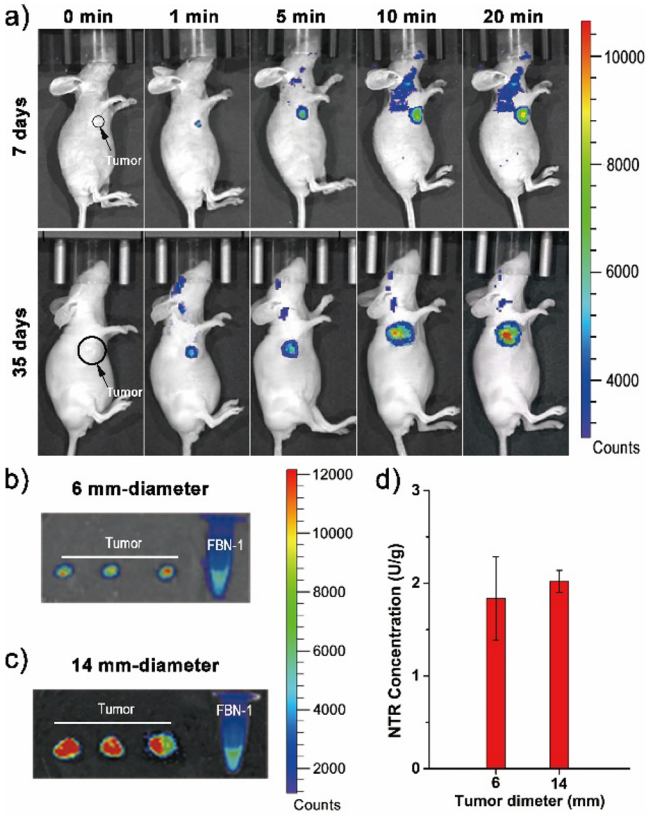

Figure 3. (a) Time-dependent *in vivo* fluorescence imaging of a HepG-2 tumor mouse model (7 days and 35 days after subcutaneous implantation of HepG-2 cells) and after intratumoral injection of the FBN-1 probe. Fluorescence imaging of (b) 7-day-old excised tumors with ~6 mm diameters, or (c) 35-day-old excised tumors with ~14 mm diameters, dissected from six independent HepG-2-tumor-carrying mice models. (d) Quantitative detection of NTR in solid tumors of different sizes with ELISA.

ing that NTR levels remain largely invariant despite tumor growth, motivating future *in vivo* studies (Figure 3d).

CONCLUSION

In summary, we have developed an NTR probe, FBN-1, that can be used to monitor different levels of hypoxic conditions in cancer cells. The probe displays a high quantum yield, high sensitivity, and high selectivity in detecting NTR in tumor cells. When tested with ELISA, we found no significant change in NTR concentrations between cancer cell samples cultured under different oxygen concentrations. Therefore, we can exclude the effect of intracellular NTR concentration on the increase in fluorescence *in vitro*. Confocal fluorescence imaging and flow cytometry demonstrated that FBN-1 can be used to monitor hypoxic conditions at the cellular level in real time. FBN-1 can also distinguish different growth stages of tumors by measuring the degree of hypoxia in tumors *in vivo*. In tumor-bearing mice, we found that NTR concentration remains nearly constant in the tumor tissue whether 7 days or 35 days post-implantation. This probe may also be used to determine the molecular mechanism underlying the malignant transformation of tumors in the absence of oxygen.

ASSOCIATED CONTENT

Supporting Information

The Supporting Information is available free of charge on the ACS Publications website at DOI: 10.1021/acssensors.7b00171.

Synthetic procedures for the intermediates of FBN-1−3; characterization data; experimental procedures; fluorescent imaging; HPLC profiles; MTT assay; flow cytometry data; ELISA experiments (PDF)

AUTHOR INFORMATION

Corresponding Authors

*E-mail: jcwu@ecust.edu.cn.

*E-mail: landry@berkeley.edu.

ORCID

Markita P. Landry: 0000-0002-5832-8522

Notes

The authors declare no competing financial interest.

ACKNOWLEDGMENTS

We thank the National Basic Research 973 Program (2013CB733700), and NSFC (91529101 and 21572057) for financial support. This work was supported by a Burroughs Wellcome Fund Career Award at the Scientific Interface (CASI), the Simons Foundation, a Stanley Fahn PDF Junior Faculty Grant with Award # PF-JFA-1760, and a Beckman Foundation Young Investigator Award (M.P.L.).

REFERENCES

(1) Brown, J. M.; Wilson, W. R. Exploiting tumour hypoxia in cancer treatment. *Nat. Rev. Cancer* **2004**, *4*, 437−447.

(2) Coleman, C. N. J. Natl. Hypoxia in tumors: a paradigm for the approach to biochemical and physiologic heterogeneity. *Cancer Inst.* **1988**, *80*, 310−317.

(3) Krishnamachary, B.; Berg-Dixon, S.; Kelly, B.; Agani, F.; Feldser, D.; Ferreira, G.; Iyer, N.; LaRusch, J.; Pak, B.; Taghavi, P.; Semenza, G. L. Regulation of colon carcinoma cell invasion by hypoxia-inducible factor 1. *Cancer Res.* **2003**, *63*, 1138−1143.

(4) Kizaka-Kondoh, S.; Inoue, M.; Harada, H.; Hiraoka, M. Tumor hypoxia: a target for selective cancer therapy. *Cancer Sci.* **2003**, *94*, 1021−1028.

(5) Rofstad, E. K.; Rasmussen, H.; Galappathi, K.; Mathiesen, B.; Nilsen, K.; Graff, B. A. Hypoxia promotes lymph node metastasis in human melanoma xenografts by up-regulating the urokinase-type plasminogen activator receptor. *Cancer Res.* **2002**, *62*, 1847−1853.

(6) Vaupel, P. Sem. Tumor microenvironmental physiology and its implications for radiation oncology. *Radiat. Oncol.* **2004**, *14*, 198−206.

(7) Chan, D. A.; Giaccia, A. J. Hypoxia, gene expression, and metastasis. *Cancer Metastasis Rev.* **2007**, *26*, 333−339.

(8) Wilson, W. R.; Hay, M. P. Targeting hypoxia in cancer therapy. *Nat. Rev. Cancer* **2011**, *11*, 393−410.

(9) Sun, X.; Niu, G.; Chan, N.; Shen, B.; Chen, X. *Mol.* Tumor hypoxia imaging. *Imaging Biol.* **2011**, *13*, 399−410.

(10) Piao, W.; Tsuda, S.; Tanaka, Y.; Maeda, S.; Liu, F.; Takahashi, S.; Kushida, Y.; Komatsu, T.; Ueno, T.; Terai, T.; Nakazawa, T.; Uchiyama, M.; Morokuma, K.; Tetsuo Nagano, T.; Kenjiro Hanaoka, K. Development of azo-based fluorescent probes to detect different levels of hypoxia. *Angew. Chem., Int. Ed.* **2013**, *52*, 13028−13032.

(11) Yu, J.; Zhang, Y.; Hu, X.; Wright, G.; Gu, Z. Hypoxia-sensitive materials for biomedical applications. *Ann. Biomed. Eng.* **2016**, *44*, 1931−1945.

(12) Feng, P.; Zhang, H.; Deng, Q.; Liu, W.; Yang, L.; Li, G.; Chen, G.; Du, L.; Ke, B.; Li, M. Real-time bioluminescence imaging of nitroreductase in mouse model. *Anal. Chem.* **2016**, *88*, 5610−5614.

DOI: 10.1021/acssensors.7b00171
ACS Sens. XXXX, XXX, XXX−XXX

(13) Okuda, K.; Okabe, Y.; Kadonosono, T.; Ueno, T.; Youssif, B. G. M.; Kizaka-Kondoh, S.; Nagasawa, H. 2-Nitroimidazole-tricarbocyanine conjugate as a near-infrared fluorescent probe for *in vivo* imaging of tumor hypoxia. *Bioconjugate Chem.* **2012**, *23*, 324−329.
(14) Xu, K.; Wang, F.; Pan, X.; Liu, R.; Ma, J.; Kong, F.; Tang, B. High selectivity imaging of nitroreductase using a near-infrared fluorescence probe in hypoxic tumor. *Chem. Commun.* **2013**, *49*, 2554−2556.
(15) Xue, C.; Lei, Y.; Zhang, S.; Sha, Y. A cyanine-derived "turn-on" fluorescent probe for imaging nitroreductase in hypoxic tumor cells. *Anal. Methods* **2015**, *7*, 10125−10128.
(16) Shi, Y.; Zhang, S.; Zhang, X. A novel near-infrared fluorescent probe for selectively sensing nitroreductase (NTR) in an aqueous medium. *Analyst* **2013**, *138*, 1952−1955.
(17) Danson, S.; Ward, T. H.; Butler, J.; Ranson, M. DT-diaphorase: a target for new anticancer drugs. *Cancer Treat. Rev.* **2004**, *30*, 437−449.
(18) Vorobyeva, A. G.; Stanton, M.; Godinat, A.; Lund, K. B.; Karateev, G. G.; Francis, K. P.; Allen, E.; Gelovani, J. G.; McCormack, E.; Tangney, M.; Dubikovskaya, E. A. Development of a bioluminescent nitroreductase probe for preclinical imaging. *PLoS One* **2015**, *10*, e0131037.
(19) Cao, J.; Campbell, J.; Liu, L.; Mason, R. P.; Lippert, A. R. *In vivo* chemiluminescent imaging agents for nitroreductase and tissue oxygenation. *Anal. Chem.* **2016**, *88*, 4995−5002.
(20) Bae, J.; McNamara, L. E.; Nael, M. A.; Mahdi, F.; Doerksen, R. J.; Bidwell, G. L., III; Hammer, N. I.; Jo, S. Nitroreductase-triggered activation of a novel caged fluorescent probe obtained from methylene blue. *Chem. Commun.* **2015**, *51*, 12787−12790.
(21) Evans, S. M.; Kim, K.; Moore, C. E.; Uddin, M. I.; Capozzi, M. E.; Craft, J. R.; Sulikowski, G. A.; Jayagopal, A. Molecular probes for imaging of hypoxia in the retina. *Bioconjugate Chem.* **2014**, *25*, 2030−2037.
(22) Wong, R. H. F.; Kwong, T.; Yau, K. H.; Au-Yeung, H. Y. Real time detection of live microbes using a highly sensitive bioluminescent nitroreductase probe. *Chem. Commun.* **2015**, *51*, 4440−4442.
(23) Huang, H. C.; Wang, K. L.; Huang, S. T.; Lin, H. Y.; Lin, Ch. M. Development of a sensitive long-wavelength fluorogenic probe for nitroreductase: A new fluorimetric indictor for analyte determination by dehydrogenase-coupled biosensors. *Biosens. Bioelectron.* **2011**, *26*, 3511−3516.
(24) Plumb, J. A.; Gerritsen, M.; Milroy, R.; Thomson, P.; Workman, P. Relative importance of DT-diaphorase and hypoxia in the bioactivation of E09 by human lung tumor cell lines. *Int. J. Radiat. Oncol., Biol., Phys.* **1994**, *29*, 295−299.
(25) Uddin, M. I.; Evans, S. M.; Craft, J. R.; Marnett, L. J.; Uddin, M. J.; Jayagopal, A. Applications of azo-based probes for imaging retinal hypoxia. *ACS Med. Chem. Lett.* **2015**, *6*, 445−449.
(26) Luo, S.; Liu, Y.; Wang, F.; Fei, Q.; Shi, B.; An, J.; Zhao, Ch.; Tung, C. A fluorescent turn-on probe for visualizing lysosomes in hypoxic tumor cells. *Analyst* **2016**, *141*, 2879−2882.
(27) Nunn, A.; Linder, K.; Strauss, H. Nitroimidazoles and imaging hypoxia W. *Eur. J. Nucl. Med.* **1995**, *22*, 265−280.
(28) Kedderis, G. L.; Miwa, G. T. The metabolic activation of nitroheterocyclic therapeutic agents. *Drug Metab. Rev.* **1988**, *19*, 33−62.
(29) Li, Z.; Li, X.; Gao, X.; Zhang, Y.; Shi, W.; Ma, H. Nitroreductase detection and hypoxic tumor cell imaging by a designed sensitive and selective fluorescent probe, 7-[(5-nitrofuran-2-yl) methoxy]-3H-phenoxazin-3-one. *Anal. Chem.* **2013**, *85*, 3926−3932.
(30) Li, Z.; Gao, X.; Shi, W.; Li, X.; Ma, H. 7-((5-Nitrothiophen-2-yl) methoxy)-3 H-phenoxazin-3-one as a spectroscopic off−on probe for highly sensitive and selective detection of nitroreductase. *Chem. Commun.* **2013**, *49*, 5859−5861.
(31) Bryant, D.; McCalla, D.; Leeksma, M.; Laneuville, P. Type I nitroreductases of *Escherichia coli*. *Can. J. Microbiol.* **1981**, *27*, 81−86.
(32) Chauviac, F. X.; Bommer, M.; Yan, J.; Parkin, G.; Daviter, T.; Lowden, P.; Raven, E. L.; Thalassinos, K.; Keep, N. L. Crystal structure of reduced MsAcg, a putative nitroreductase from Mycobacterium smegmatis and a close homologue of mycobacterium tuberculosis Acg[J]. *J. Biol. Chem.* **2012**, *287* (53), 44372−44383.
(33) Somerville, C. C.; Nishino, S. F.; Spain, J. C. Purification and characterization of nitrobenzene nitroreductase from Pseudomonas pseudoalcaligenes JS45[J]. *J. Bacteriol.* **1995**, *177* (13), 3837−3842.
(34) Xiao, Y.; Wu, J. F.; Liu, H.; Wang, S. J. Characterization of genes involved in the initial reactions of 4-chloronitrobenzene degradation in pseudomonasputida ZWL73[J]. *Appl. Microbiol. Biotechnol.* **2006**, *73* (1), 166−171.
(35) Li, Z.; He, X.; Wang, Z.; Yang, R.; Shi, W.; Ma, H. *In vivo* imaging and detection of nitroreductase in zebrafish by a new near-infrared fluorescence off−on probe. *Biosens. Bioelectron.* **2015**, *63*, 112−116.
(36) Wan, Q. Q.; Gao, X. H.; He, X. Y.; Chen, S. M.; Song, Y. C.; Gong, Q. Y.; Li, X.; Ma, H. A Cresyl Violet-Based Fluorescent off−on probe for the detection and imaging of hypoxia and nitroreductase in living organisms. *Chem. - Asian J.* **2014**, *9*, 2058−2062.
(37) Guo, T.; Cui, L.; Shen, J.; Zhu, W.; Xu, Y.; Qian, X. A. Highly sensitive long-wavelength fluorescence probe for nitroreductase and hypoxia: selective detection and quantification. *Chem. Commun.* **2013**, *49*, 10820−10822.
(38) Yuan, J.; Xu, Y.-Q.; Zhou, N.-N.; Wang, R.; Qian, X.-H.; Xu, Y.-F. A highly selective turn-on fluorescent probe based on semi-cyanine for the detection of nitroreductase and hypoxic tumor cell imaging. *RSC Adv.* **2014**, *4*, 56207−56210.
(39) Cui, L.; Zhong, Y.; Zhu, W.; Xu, Y.; Du, Q.; Wang, X.; Qian, X.; Xiao, Y. A new prodrug-derived ratiometric fluorescent probe for hypoxia: high selectivity of nitroreductase and imaging in tumor cell. *Org. Lett.* **2011**, *13*, 928−931.
(40) Zhang, J.; Liu, H.; Hu, X.; Li, J.; Liang, L.; Zhang, X.; Tan, W. Efficient two-photon fluorescent probe for nitroreductase detection and hypoxia imaging in tumor cells and tissues. *Anal. Chem.* **2015**, *87*, 11832−11839.
(41) Li, Y.; Sun, Y.; Li, J.; Su, Q.; Yuan, W.; Dai, Y.; Han, C.; Wang, Q.; Feng, W.; Li, F. Ultrasensitive near-infrared fluorescence-enhanced probe for *in vivo* nitroreductase imaging. *J. Am. Chem. Soc.* **2015**, *137*, 6407−6416.
(42) Witek, M. A.; Wei, S.; Vaidya, B.; Adams, A. A.; Zhu, Li.; Stryjewski, W.; McCarley, R. L.; Soper, S. A. Cell transport via electromigration in polymer-based microfluidic devices. *Lab Chip* **2004**, *4*, 464−472.
(43) Kawaguchi, M.; Okabe, T.; Okudaira, S.; Hanaoka, K.; Fujikawa, Y.; Terai, T.; Komatsu, T.; Kojima, H.; Aoki, J.; Nagano, T. Fluorescence probe for lysophospholipase C/NPP6 activity and a potent NPP6 inhibitor. *J. Am. Chem. Soc.* **2011**, *133*, 12021−12030.
(44) Kobayashi, T.; Urano, Y.; Kamiya, M.; Ueno, T.; Kojima, H.; Nagano, T. Highly activatable and rapidly releasable caged fluorescein derivatives. *J. Am. Chem. Soc.* **2007**, *129*, 6696−66.
(45) Nudo, L. P.; Catap, E. S. Anti-immunosuppressive effects of Chromolaena odorata (Lf.) King & Robinson (Asteraceae) leaf extract in cyclophosphamide-injected Balb/C mice[J]. *Philipp. J. Sci.* **2012**, *141* (1), 35−43.
(46) Chaisowwong, W.; Kusumoto, A.; Hashimoto, M.; Harada, T.; Maklon, K.; Kawamoto, K. Physiological characterization of Campylobacter jejuni under cold stresses conditions: its potential for public threat[J]. *J. Vet. Med. Sci.* **2012**, *74* (1), 43−50.
(47) Zhu, D.; Xue, L.; Li, G.; Jiang, H. A highly sensitive near-infrared ratiometric fluorescent probe for detecting nitroreductase and cellular imaging[J]. *Sens. Actuators, B* **2016**, *222*, 419−424.
(48) Chevalier, A.; Zhang, Y.; Khdour, O. M.; Kaye, J. B.; Hecht, S. M. Mitochondrial Nitroreductase Activity Enables Selective Imaging and Therapeutic Targeting. *J. Am. Chem. Soc.* **2016**, *138*, 12009−12012.

DOI: 10.1021/acssensors.7b00171
ACS Sens. XXXX, XXX, XXX−XXX